# Electrochemical Surface Analysis of LiMnO Thin-film Electrodes in LiPF6/Propylene Carbonate at Room and Elevated Temperatures

AUTHOR(S):

INAMOTO, Junichi; FUKUTSUKA, Tomokazu; MIYAZAKI, Kohei; ABE, Takeshi

CITATION:

INAMOTO, Junichi ...[et al]. Electrochemical Surface Analysis of LiMnO Thin-film Electrodes in LiPF6/Propylene Carbonate at Room and Elevated Temperatures. Electrochemistry 2021, 89(1): 19-24

ISSUE DATE:

2021-01

URL:

http://hdl.handle.net/2433/277794

Electrochemistry
The Electrochemical Society of Japan
Received: September 9, 2020
Accepted: October 6, 2020
Published online: October 15, 2020
https://doi.org/10.5796/electrochemistry.20-00112
Article
*Electrochemistry*, **89(1)**, 19–24 (2021)

# Electrochemical Surface Analysis of $LiMn_2O_4$ Thin-film Electrodes in $LiPF_6$/Propylene Carbonate at Room and Elevated Temperatures

**Junichi INAMOTO,[a,†*] Tomokazu FUKUTSUKA,[a,‡] Kohei MIYAZAKI,[a,b] and Takeshi ABE[a,b]**

[a] *Graduate School of Engineering, Kyoto University, Kyoto daigaku-katsura, Nishikyo-ku, Kyoto 615-8510, Japan*
[b] *Hall of Global Environmental Research, Kyoto University, Kyoto daigaku-katsura, Nishikyo-ku, Kyoto 615-8510, Japan*

* *Corresponding author: j.inamoto@eng.u-hyogo.ac.jp*

**ABSTRACT**

Degradation of $LiMn_2O_4$ in $LiPF_6$-based electrolyte solution is complicated due to the influence of $PF_6^-$ anion. Decomposition of $PF_6^-$ anion accelerates both of dissolution of manganese ion and surface-film formation. In this study, surface states of $LiMn_2O_4$ thin-film electrodes in $LiPF_6$/propylene carbonate (PC) derived from the surface-film formation were investigated using redox reaction of ferrocene and spectroscopic analyses. The spectroscopic analyses suggested that properties of the surface film depended the operation temperature (30 °C and 55 °C); a thinner surface film composed of LiF and PC decomposition products formed on $LiMn_2O_4$ at 30 °C and a thicker surface film was formed at 55 °C. The redox reaction of ferrocene clearly showed that $LiMn_2O_4$ was completely passivated at 30 °C, while it was partially passivated at 55 °C, indicating the surface film formed at 55 °C was not compact and $LiMn_2O_4$ was exposed to the electrolyte solution. It was one of the causes of the rapid degradation of $LiMn_2O_4$ at elevated temperatures in $LiPF_6$-based electrolyte solution.



Keywords : Lithium-ion Batteries, $LiMn_2O_4$, Surface Film, Degradation

## 1. Introduction

Recent advancement in lithium-ion batteries (LIBs) technology has enabled practical use of electric vehicles (EVs). Since the energy density of the LIB determines the cruising distance of the EV, the LIB with high energy density is required. In addition, they are also required low cost and high reliability to avoid thermal run away. Concerning these required features, $LiMn_2O_4$ is one of the most attractive materials for positive electrode because manganese is relatively abundant transition metal and the material is thermally stable. Therefore, the material has been widely used in LIBs for EVs. Although $LiMn_2O_4$ shows such ideal properties, it suffers from severe capacity fading during its operation especially at elevated temperatures,[1–5] which is a crucial shortcoming for long-term use of the LIBs.

Thus far, degradation mechanisms of $LiMn_2O_4$ have been extensively studied for over two decades, and various degradation phenomena such as Jahn–Teller distortion,[6–8] dissolution of manganese ion,[1–5,9–13] structural changes[3–5,10,14–17] and surface film formation[15,17–29] have been reported. In particular, the dissolution is the most severe problem for $LiMn_2O_4$. In the practical LIBs, $LiPF_6$ has been commonly used as a lithium salt. However, $PF_5$, decomposition products of $PF_6^-$ anion, reacts with impurity water in the solution to form HF, which accelerates the dissolution of manganese ion.[2–5,9] In addition, the surface-film formation is also a severe problem in $LiPF_6$-based electrolyte solution because $F^-$ forms LiF, which has low conductivity of lithium-ion, on the surface of $LiMn_2O_4$.[15,17–22,29] Moreover, since $PF_5$ is a strong Lewis acid, it triggers polymerization of organic solvent to form organic surface film, resulting in large interfacial resistance.[30–32] Furthermore, these degradation phenomena brought by $LiPF_6$ are accelerated at elevated temperature because of thermal instability of $LiPF_6$. For these reasons, the degradation mechanism at the surface region of $LiMn_2O_4$ in $LiPF_6$-based electrolyte solution should be quite complicated.

Since the dissolution of manganese ion and formation of the surface film competitively occur, these processes possibly influence on each other. Hirayama et al. reported that the compact surface film formed in $LiPF_6$-based electrolyte solution protected the surface of $LiMn_2O_4$ from attack by HF, resulting in suppression of dissolution of manganese ion.[17] In addition, it was also suggested that non-uniform surface film did not completely suppress the degradation of $LiMn_2O_4$.[17] This study clearly showed that the properties of the surface film affected the other degradation phenomena occurring at the surface region of $LiMn_2O_4$. Based on this suggestive study, it is considered that the compact surface film which uniformly covers $LiMn_2O_4$ is ideal for protecting it from the side reactions. Thus far, a large number of surface analyses of $LiMn_2O_4$ were conducted using X-ray photoelectron spectroscopy (XPS), which is one of the most powerful tools for the surface analysis. However, since an area of X-ray beam spot is larger than micrometer scale, it was not suitable to analyze the compactness of the surface film along the in-plane direction. Since the side reactions takes place at the interface between $LiMn_2O_4$ and electrolyte solution, it is important to analyze the surface in much smaller scale. In general, there are few spectroscopic methods which can analyze the surface region of the sample in such scale. As for microscopic analysis such as transmission electron microscope (TEM), the surface region of the sample can be analyzed in atomic scale. However, since TEM is conducted after pre-treatment of the sample in high vacuum condition, it is difficult to observe fragile or volatile components in the surface film.

Therefore, in this study, we employed redox reaction of ferrocene as a probe for surface analysis of $LiMn_2O_4$. In our previous study, it was investigated that the surface-film formation behavior on the $LiMn_2O_4$ thin-film electrode in $LiClO_4$/propylene carbonate (PC) using redox reaction of ferrocene.[33] As the result, it was clarified that

†Current affiliation: Graduate School of Engineering, University of Hyogo, 2167, Shosha, Himeji 671-2280, Japan
‡Current affiliation: Graduate School of Engineering, Nagoya University, Furo-cho, Chikusa-ku, Nagoya 464-8603, Japan

the electronic passivation of the electrodes did not occur during charge–discharge cycles at room temperature, and it occurred only at elevated temperature. Using this method, the coverage of the surface film formed in $LiPF_6$-based electrolyte solution can be discussed in much smaller scale than XPS. In order to investigate the effect of operating temperature on the surface states of $LiMn_2O_4$, the cycling test was carried out at 30 °C and 55 °C. Analyzing the changes in the surface state of $LiMn_2O_4$ thin-film electrodes during cycling using redox reaction of ferrocene together with spectroscopic analyses, the degradation phenomena at the surface region of $LiMn_2O_4$ was investigated.

## 2. Experimental

### 2.1 Preparation of $LiMn_2O_4$ thin-film electrode

$LiMn_2O_4$ thin-film electrodes were prepared by pulsed laser deposition (PLD) method using the fourth harmonic of Nd: YAG laser (Electronics Optic Research Ltd.). The energy density of the laser beam was set at 1.08 J cm$^{-2}$. The repetition frequency was 10 Hz. $Li_{1.4}Mn_2O_{4+x}$ was used as a target material. The chamber pressure was kept at 27 Pa by flowing $O_2$ gas during the deposition. The thin film was prepared on a mirror-polished platinum substrate heated at 873 K for 1 h. The resulting thin film was characterized with X-ray diffraction measurement and Raman spectroscopy.

### 2.2 Electrochemical measurements and spectroscopic analysis

Using the $LiMn_2O_4$ thin-film electrode as a working electrode, three-electrode cell was composed for electrochemical measurements. As a reference and a counter electrode, lithium metal was employed. Hereafter, all potentials are referenced to $Li^+/Li$. Lithium-ion extraction/insertion reaction was conducted by cyclic voltammetry in 1 mol dm$^{-3}$ $LiPF_6$/PC (lithium battery grade, purchased from KISHIDA CHEMICAL Co., Ltd.) at 0.1 mV s$^{-1}$ in the range of 3.5–4.2 V at 30 °C and 55 °C. Redox reaction of ferrocene was conducted in 1 mol dm$^{-3}$ $LiClO_4$/PC (Tomiyama Pure Chemical Industries, Ltd.) containing 1 mmol dm$^{-3}$ ferrocene (Alfa Aesar, purity 99 %). Cyclic voltammetry of ferrocene was carried out at 10 mV s$^{-1}$ in the range of 3.0–3.6 V at 30 °C before and after the 1st, 5th, 10th, and 20th lithium-ion extraction/insertion reaction. In addition, the electrochemical impedance spectroscopy (EIS) was conducted at 4.1 V before and after the cyclic voltammetry for the lithium-ion extraction/insertion reaction. Applied ac voltage and frequency range were set at 15 mV and 100 kHz–10 mHz. All the electrochemical measurements were conducted in argon filled glove box using HSV-100 (HOKUTO-DENKO) or Solartron1470E + 1255 (Solartron Analytical).

To evaluate redox behavior of ferrocene quantitatively, electrochemical surface area $A$ and a standard rate constant $k^0$ between ferrocene and electrode at each cycle were obtained by fitting a simulated voltammogram to the experimental one. The simulation procedure was followed to the literature,[34] and the simulation condition was shown in our previous work.[33] Modifying $k^0$ and $A$ until the simulated voltammogram fitted to the experimental ones, these values were obtained.

As the structural characterization after the lithium-ion extraction/insertion reaction, Raman spectroscopy, attenuated total reflection Fourier transform infrared spectroscopy (ATR FT-IR), and XPS measurement were conducted. Raman spectroscopy was measured with a triple monochromator (Jobin-Yvon, T64000) equipped with a CCD detector. As a light source, 514.5-nm line of argon ion laser (CVI Melles Griot, 543-GS-A03) was used. ATR FT-IR was conducted with Bruker Alpha in Ar-filled glove box. XPS measurements were carried out ex-situ with MT-5500 (ULVAC PHI, Inc.). Prior to XPS analysis, the cell was deconstructed in Ar-filled glove box to obtain cycled electrodes, and the electrodes were transferred in Ar-filled vessel to side chamber of the XPS instrument.

## 3. Results and Discussion

### 3.1 Characterization of a $LiMn_2O_4$ thin film prepared with PLD

Figure 1 shows XRD pattern of a $LiMn_2O_4$ thin film prepared with PLD. All the peaks were consistent with reported ones in previous reports,[5] and no other peak was observed. In addition, relative peak intensities were similar to those of powder one, indicating that the film did not have any specific crystalline orientation. It also suggested that the film was composed of polycrystalline $LiMn_2O_4$. Therefore, using this thin film as an electrode, the information independent from crystalline orientation at the surface can be obtained.

Figure 2 shows Raman spectrum of the thin film. Peaks around 500, 580, and 625 cm$^{-1}$ were attributed to $F_{2g}$, $F_{2g}$ and $A_{1g}$ modes of $LiMn_2O_4$, respectively.[8] Since no other peak was observed in the spectrum, the thin film was composed only of $LiMn_2O_4$ and did not contain impurity phase. From the results of XRD and Raman spectroscopy, it was found that the prepared $LiMn_2O_4$ thin film was desirable for a model electrode.

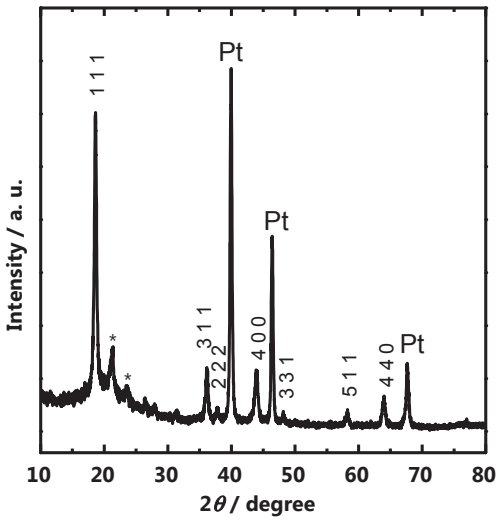


**Figure 1.** X-ray diffraction pattern of a prepared thin film on Pt substrate. Number on peaks denotes index *hkl*. * indicates peaks of sample holder.

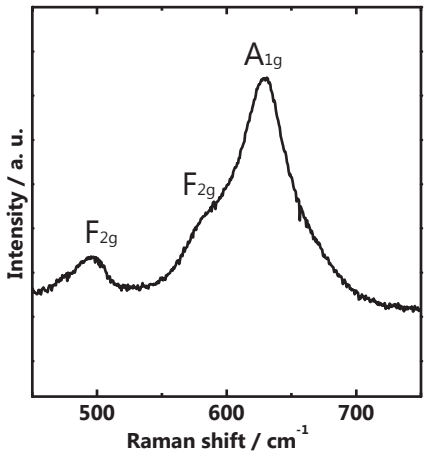


**Figure 2.** Raman spectrum of a prepared thin film.

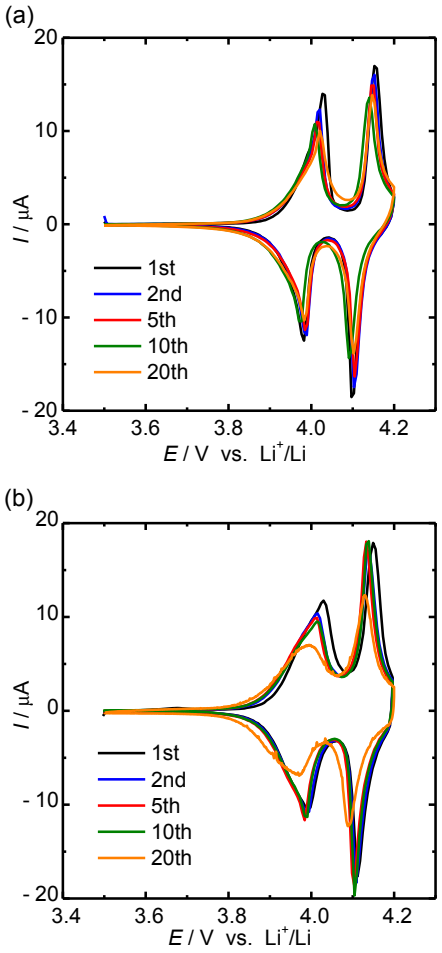


**Figure 3.** Cyclic voltammograms of $LiMn_2O_4$ thin-film electrodes in 1 mol dm$^{-3}$ $LiPF_6$/PC at 30 °C (a) and 55 °C (b).

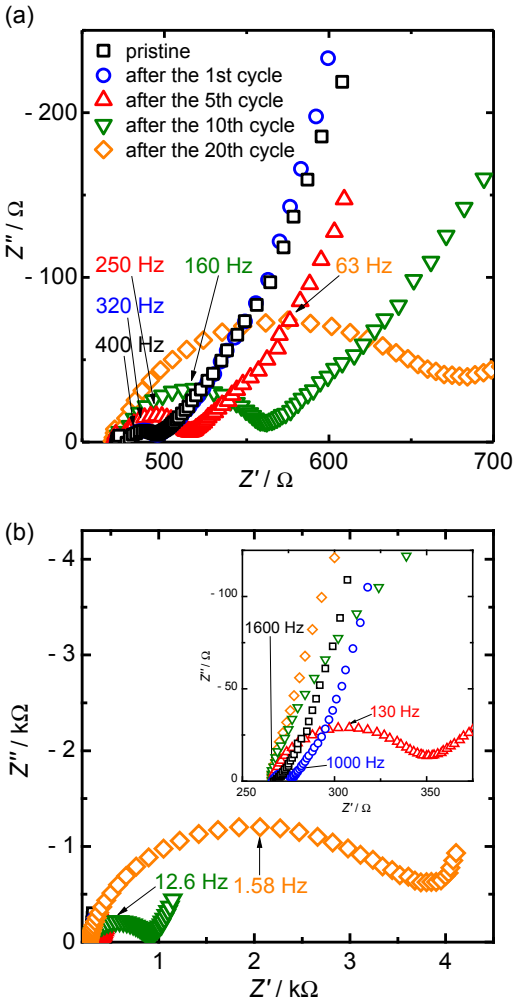


**Figure 4.** Nyquist plots of $LiMn_2O_4$ thin-film electrodes at 4.1 V vs. $Li^+$/Li during cycling in 1 mol dm$^{-3}$ $LiPF_6$/PC at 30 °C (a) and 55 °C (b). An enlarged view is inserted in (b). The value indicates the frequency at the top of the semi-circles.

### 3.2 Electrochemical properties of $LiMn_2O_4$ thin-film electrodes

Figure 3 shows cyclic voltammograms of the $LiMn_2O_4$ thin-film electrodes in 1 mol dm$^{-3}$ $LiPF_6$/PC at 30 °C and 55 °C. Around 4.0 and 4.15 V, two reversible peaks which are unique to $LiMn_2O_4$ were observed in each voltammogram. At 30 °C, peak current gradually decreased with increasing cycle number. This result was slightly different from the results in $LiClO_4$/PC of our previous report.[33] Therefore, it indicated that the degradation of $LiMn_2O_4$ was accelerated in $LiPF_6$/PC even at room temperature. At 55 °C, the peak current decreased more rapidly, indicating that the degradation of $LiMn_2O_4$ was accelerated at the elevated temperature. Many reports suggested that $LiMn_2O_4$ suffered from severe capacity fading in $LiPF_6$/PC at elevated temperatures.[1–5,35] The present result was in good agreement with these reports.

Figure 4 shows the Nyquist plots of the $LiMn_2O_4$ thin-film electrode at 30 °C and 55 °C. A semi-circle and a following straight line were observed in each Nyquist plot. The semi-circle was attributed to charge-transfer (lithium-ion transfer) resistance $R_{ct}$ at the electrode/electrolyte interface, and the straight line was assigned to lithium-ion diffusion in $LiMn_2O_4$.[36] In the both Nyquist plots, the diameters of the semi-circles increased with increasing the cycle number. For $LiMn_2O_4$ cycled at 30 °C, $R_{ct}$ increased by a factor of 15 during 20 cycles. In addition, small semi-circles were also observed at high frequency region in the plots. This semi-circle possibly attributed to lithium-ion transfer in surface layer on $LiMn_2O_4$ (note that the pristine $LiMn_2O_4$ was charged to 4.1 V to conduct EIS measurement, and surface film might be formed during the process). On the other hand, $R_{ct}$ increased by a factor of ca. 3000 during 20 cycles at 55 °C, which was much larger increasing rate than that obtained at 30 °C. The results possibly suggests that a large number of the active sites decreased during the cycling process at 55 °C, which was consistent with the variations of cyclic voltammograms. The decrement of the active sites would be discussed in detail based on the results of redox reaction of ferrocene and X-ray photoelectron spectroscopy in the next sections.

### 3.3 Redox reaction of ferrocene on $LiMn_2O_4$ thin-film electrodes

Since the degradation behaviors of $LiMn_2O_4$ thin-film electrodes remarkably depended on the operation temperatures in $LiPF_6$/PC, the surface state of the $LiMn_2O_4$ thin-film electrodes at the temperatures were investigated with the redox reaction of ferrocene. Figure 5 shows the cyclic voltammograms of ferrocene on the $LiMn_2O_4$ thin-film electrodes. Before the 1st cycle of the lithium-ion extraction/insertion, clear reversible peaks of ferrocene were observed. At 30 °C, the peaks completely disappeared after the 1st cycle. In the case at 55 °C, although the peak currents decreased after the 1st cycle, the peaks were still slightly observable even after the 20th cycle. The standard rate constant $k^0$ and ratio of the surface area to the initial value $A/A_0$ were evaluated by fitting the simulated voltammograms to the experimental ones, and they were summarized in Table 1. At 30 °C, $A/A_0$ could not be evaluated because the

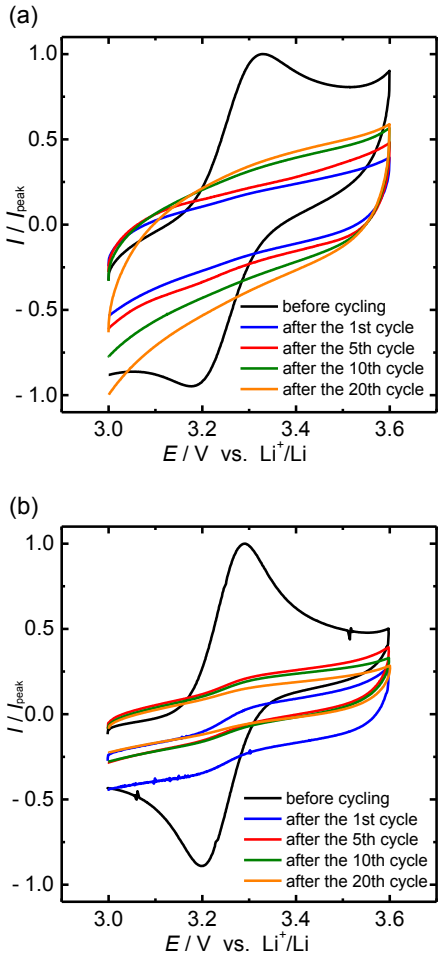


**Figure 5.** Cyclic voltammograms of redox reaction of ferrocene on $LiMn_2O_4$ thin-film electrodes during cycling in 1 mol dm$^{-3}$ $LiPF_6$/PC at 30 °C (a) and 55 °C (b).

peaks completely disappeared. After the 1st cycle, $k^0$ drastically decreased by a factor of almost one thousand at 30 °C, indicating complete electronic passivation of the $LiMn_2O_4$ thin-film electrode. Therefore, it was suggested that the film compactly covered the surface. It might suppress side reactions such as oxidation of electrolyte solution and $H^+$ attack to $LiMn_2O_4$, resulting in contribution to capacity retention. However, since the increase of $R_{ct}$ was observed in Nyquist plots at 30 °C, it was suggested that the surface film also decreased the number of the reaction sites for lithium-ion transfer at the electrode/electrolyte interface. In contrast, at 55 °C, $A/A_0$ drastically decreased after the 1st cycle, whereas $k^0$ kept similar values to the pristine one. It indicated that $LiMn_2O_4$ was not completely electronically passivated. There were two possible causes for the incomplete passivation of $LiMn_2O_4$; one is a part of $LiMn_2O_4$ was not covered by the surface film, and the other is exposure of platinum substrate resulted from massive dissolution of manganese ion. However, if platinum substrate was exposed by the dissolution of $LiMn_2O_4$, the redox current of the ferrocene must increase with increasing the cycling number. In Fig. 5(b), the redox current decreased with increasing the cycle number. Therefore, it is considered that the surface film formed at 55 °C did not completely cover the surface and a slight part of the surface was still exposed to the electrolyte solution. The incomplete formation of the surface film would be caused by the harsh dissolution of manganese ion at the elevated temperature. During the following cycles, the value of $A/A_0$ continuously decreased, indicating that the surface film grew after the 1st cycle and the exposed area of $LiMn_2O_4$ gradually

**Table 1.** Ratio of surface area to the initial value $A/A_0$ and standard rate constant $k^0$ between ferrocene and $LiMn_2O_4$ thin-film electrodes.

| number of cycle | 30 °C | 55 °C | |
|---|---|---|---|
| | $k^0$/cm s$^{-1}$ | $k^0$/cm s$^{-1}$ | $A/A_0$ |
| 0 | $6.5 \times 10^{-4}$ | $2.0 \times 10^{-3}$ | 1.0 |
| 1 | $<3.1 \times 10^{-7}$ | $1.7 \times 10^{-3}$ | $9.6 \times 10^{-2}$ |
| 5 | $<3.1 \times 10^{-7}$ | $2.1 \times 10^{-3}$ | $7.2 \times 10^{-2}$ |
| 10 | $<3.1 \times 10^{-7}$ | $1.7 \times 10^{-3}$ | $7.6 \times 10^{-2}$ |
| 20 | $<3.1 \times 10^{-7}$ | $1.7 \times 10^{-3}$ | $3.4 \times 10^{-2}$ |

decreased during cycling. It should be the reason of the continuous increase of $R_{ct}$ observed in EIS. The present results are consistent with the previous report in terms of the thickness of the surface film after the prolonged cycles.[20] Since the surface film did not completely cover the surface of $LiMn_2O_4$ at the elevated temperature, side reactions such as further oxidation of electrolyte solution and $H^+$ attack to $LiMn_2O_4$ possibly occurred at the exposed area of $LiMn_2O_4$. It should be one of the reasons that capacity fading of $LiMn_2O_4$ rapidly and continuously proceeded at elevated temperatures.

### 3.4 Characterization of surface species on $LiMn_2O_4$ after cycling in $LiPF_6$/PC

To investigate the surface-state changes before and after the cycles, $LiMn_2O_4$ thin-film electrodes were analyzed with Raman spectroscopy, XPS and ATR FT-IR. Figure 6 shows Raman spectra of pristine and cycled $LiMn_2O_4$ thin-film electrodes. No new peak emerged after cycling, indicating other impurity phase did not exist in the $LiMn_2O_4$ thin-film electrodes. In our previous report, a new peak of $Mn_2O_3$ at 650 cm$^{-1}$ was observed for $LiMn_2O_4$ cycled in $LiClO_4$/PC at 55 °C. However, the peak was not observed in the present results in $LiPF_6$/PC. It was reported that $Mn_2O_3$ was easily dissolved into $LiPF_6$-based electrolyte solution at elevated temperature.[3] Therefore, $Mn_2O_3$ might be once formed on $LiMn_2O_4$ at 55 °C in $LiPF_6$/PC, but it immediately dissolved into $LiPF_6$/PC. This may be the reason of no observation of $Mn_2O_3$. It should be emphasized that structural change at the surface region of $LiMn_2O_4$ was not the reason of the increase of $R_{ct}$.

Figure 7 shows the depth profiles of the atomic concentrations at the surface region of pristine and cycled $LiMn_2O_4$ thin-film electrodes calculated from the results of XPS. In both profiles of cycled $LiMn_2O_4$, a large concentration of Li and F were observed at

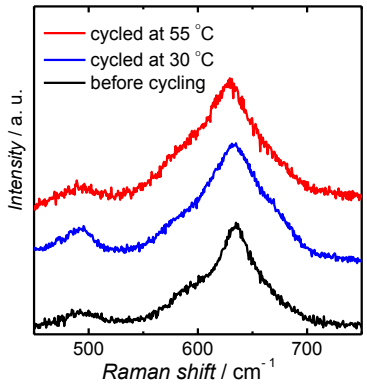


**Figure 6.** Raman spectra of $LiMn_2O_4$ thin-film electrodes before cycling and after the 20th cycle in 1 mol dm$^{-3}$ $LiPF_6$/PC at 30 °C and 55 °C.

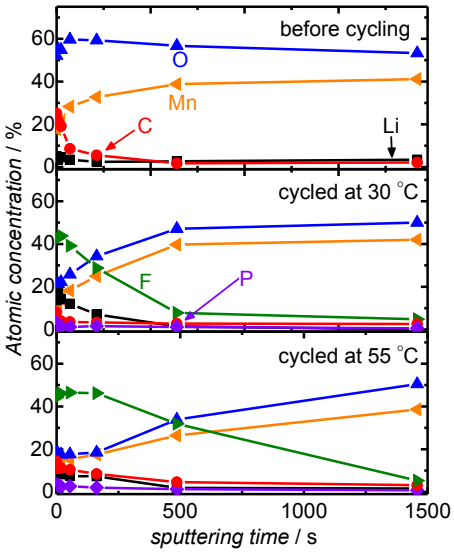


**Figure 7.** Depth profile of $LiMn_2O_4$ thin-film electrodes before cycling and after the 5th cycle in 1 mol dm$^{-3}$ $LiPF_6$/PC at 30 °C and 55 °C evaluated from the results of X-ray photoelectron spectroscopy.

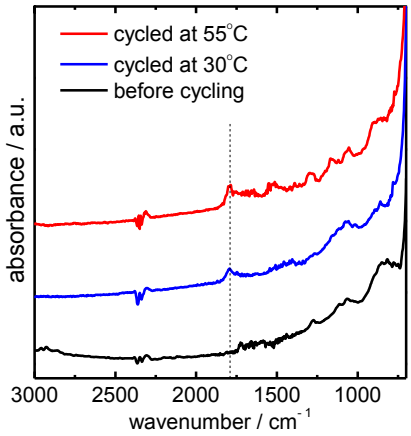


**Figure 8.** Attenuated total reflection Fourier transform infrared spectra of $LiMn_2O_4$ thin-film electrodes before cycling and after the 5th cycle in 1 mol dm$^{-3}$ $LiPF_6$/PC at 30 °C and 55 °C.

short sputtering time. Since the $LiMn_2O_4$ cycled at 55 °C showed higher concentrations of Li and F at 486-s sputtering, the thicker LiF was formed on the surface. The results clearly indicated that the thickness of the LiF surface film increased with increasing temperature, and it is in good agreement with the previous report on surface film on $LiMn_2O_4$.[20] In addition, C and a slight amount of P were also observed, which were attributed to decomposition products of PC and $PF_6^-$, respectively. Comparing variations of C and F in depth profile, concentration of F kept almost the same value during 162 s of sputtering, while that of C gradually decreased. It indicated that organic species derived from PC was formed on top surface of the electrode, and LiF was formed near the surface of $LiMn_2O_4$. Since the formation of LiF on $LiMn_2O_4$ decrease active sites for lithium-ion extraction and insertion, it could cause the large increase of $R_{ct}$ observed in EIS.

In addition to XPS, ATR FT-IR was conducted to analyze organic species on the surface of $LiMn_2O_4$. Figure 8 shows the ATR FT-IR spectra of the pristine $LiMn_2O_4$ and $LiMn_2O_4$ after the 5th cycle at 30 °C and 55 °C. For the both cycled $LiMn_2O_4$, new peaks around 1780 cm$^{-1}$ appeared. According to the report by Matsui et al., C=O double bond in decomposition products of PC showed peak at 1780 cm$^{-1}$.[37] Therefore, decomposition products of PC precipitated on the surface of the cycled $LiMn_2O_4$. In our previous study, surface film derived from decomposition products of PC was not observed on $LiMn_2O_4$ cycled in $LiClO_4$/PC at 30 °C in FT-IR spectrum. In contrast, in the present results, the organic surface film was observed at 30 °C in $LiPF_6$/PC. It was reported that $PF_5$, decomposition products of $LiPF_6$, was a strong Lewis acid and acted as an initiator of polymerization of carbonates.[30,32] Therefore, such a difference in formation of PC-decomposition products at 30 °C was possibly resulted from instability of $PF_6^-$ anion. As for decomposition products of $PF_6^-$, no peak corresponding to them were observed in the spectra. However, it does not follow that the result denies the formation of the surface species derived from the decomposition products of $PF_6^-$. Since total amount of the surface film formed on the thin-film electrode should be smaller than that formed in composite electrodes, it might be difficult to detect the minor species with FT-IR. From the result of XPS, there was a slight amount of P atom on the surface region. Therefore, there should be a small amount of the species from $PF_6^-$ on the surface.

From these results, the surface states of $LiMn_2O_4$ in $LiPF_6$/PC were summarized as follows. After the cycling at 30 °C, $LiMn_2O_4$ was covered with the compact surface film composed of LiF and PC-decomposition products, and it led to complete passivation of $LiMn_2O_4$. In this regard, the surface film contributed to suppression of further side reactions such as the dissolution of manganese ion to a certain extent. However, since the charge-transfer resistance also largely increased by the surface film, the film also hindered interfacial lithium-ion transfer. In our previous report,[33] it was revealed that the surface film derived from PC hardly hindered the interfacial lithium-ion transfer. Therefore, such low lithium-ion conductivity of the surface film was caused by LiF, which is known as a poor lithium-ion conductor. At 55 °C, although the thicker surface film was formed, it was not compact and $LiMn_2O_4$ was partially exposed to the electrolyte solution. It was probably because the emission of HF was accelerated at the elevated temperature and dissolution of manganese ion rapidly proceeded. The continuous dissolution of manganese ion occurred at the exposed area of $LiMn_2O_4$, preventing from formation of compact surface film, and resulted in severe capacity degradation of $LiMn_2O_4$. It is, namely, a vicious cycle of surface degradation. This shows marked contrast to the surface state of $LiMn_2O_4$ in $LiClO_4$/PC at 55 °C.[33] The surface film formed in $LiClO_4$/PC completely electronically passivated $LiMn_2O_4$ and it prevented $LiMn_2O_4$ from the interfacial side reactions during cycling. The contrast clearly showed the intrinsic difficulties of $LiPF_6$-based electrolyte solution for long-term cycling of $LiMn_2O_4$. Even at 30 °C, the interfacial lithium-ion transfer was much slower because of the low lithium-ion conductive surface film. In addition, at 55 °C, the surface film could not suppress the severe interfacial side reactions. Although $LiPF_6$ is widely used in commercialized LIBs, alternative electrolytes which are safe and stable are required for further improvement of the long-term cycleability of the LIBs.

## 4. Conclusion

The electronic passivation behavior of $LiMn_2O_4$ cycled in $LiPF_6$/PC was strongly influenced by its operation temperature; At 30 °C, complete electronic passivation was brought by compact surface film composed of LiF and decomposition products of PC. The electronic passivation possibly suppressed further side reactions at the interface such as dissolution of manganese ion and oxidation of electrolyte solution, leading to suppression of capacity fading. However, it also hindered interfacial lithium-ion transfer, resulting in worse rate capability. On the other hand, at 55 °C, the surface film

was thick but not compact, and it did not completely electronically passivate $LiMn_2O_4$. Therefore, $LiMn_2O_4$ was partially exposed to the electrolyte solution, and further side reactions such as dissolution of manganese ion continuously occurred during cycling, leading to instability of the surface film. This vicious cycle of surface degradation should be one of the causes of rapid degradation of $LiMn_2O_4$ at elevated temperatures.

## References

1. R. J. Gummow, A. d. Kock, and M. M. Thackeray, *Solid State Ionics*, **69**, 59 (1994).
2. D. H. Jang, Y. J. Shin, and S. M. Oh, *J. Electrochem. Soc.*, **143**, 2204 (1996).
3. Y. Xia, Y. Zhou, and M. Yoshio, *J. Electrochem. Soc.*, **144**, 2593 (1997).
4. T. Inoue and M. Sano, *J. Electrochem. Soc.*, **145**, 3704 (1998).
5. D. Aurbach, M. D. Levi, K. Gamulski, B. Markovsky, G. Salitra, E. Levi, U. Heider, L. Heider, and R. Oesten, *J. Power Sources*, **81**, 472 (1999).
6. A. Yamada and M. Tanaka, *Mater. Res. Bull.*, **30**, 715 (1995).
7. G. G. Amatucci, C. N. Schmutz, A. Blyr, C. Sigala, A. S. Gozdz, D. Larcher, and J. M. Tarascon, *J. Power Sources*, **69**, 11 (1997).
8. C. M. Julien and M. Massot, *Mater. Sci. Eng., B*, **97**, 217 (2003).
9. J. C. Hunter, *J. Solid State Chem.*, **39**, 142 (1981).
10. A. Blyr, C. Sigala, G. Amatucci, D. Guyomard, Y. Chabre, and J.-M. Tarascon, *J. Electrochem. Soc.*, **145**, 194 (1998).
11. D. H. Jang and S. M. Oh, *J. Electrochem. Soc.*, **144**, 3342 (1997).
12. T. Uchiyama, M. Nishizawa, T. Itoh, and I. Uchida, *J. Electrochem. Soc.*, **147**, 2057 (2000).
13. L.-F. Wang, C.-C. Ou, K. A. Striebel, and J.-S. Chen, *J. Electrochem. Soc.*, **150**, A905 (2003).
14. J. Cho and M. M. Thackeray, *J. Electrochem. Soc.*, **146**, 3577 (1999).
15. Y. Matsuo, R. Kostecki, and F. McLarnon, *J. Electrochem. Soc.*, **148**, A687 (2001).
16. G. Li, Y. Iijima, Y. Kudo, and H. Azuma, *Solid State Ionics*, **146**, 55 (2002).
17. M. Hirayama, H. Ido, K. S. Kim, W. Cho, K. Tamura, J. Mizuki, and R. Kanno, *J. Am. Chem. Soc.*, **132**, 15268 (2010).
18. D. Aurbach, K. Gamolsky, B. Markovsky, G. Salitra, Y. Gofer, U. Heider, R. Oesten, and M. Schmidt, *J. Electrochem. Soc.*, **147**, 1322 (2000).
19. T. Eriksson, A. M. Andersson, A. G. Bishop, C. Gejke, T. Gustafsson, and J. O. Thomas, *J. Electrochem. Soc.*, **149**, A69 (2002).
20. T. Eriksson, A. M. Andersson, C. Gejke, T. Gustafsson, and J. O. Thomas, *Langmuir*, **18**, 3609 (2002).
21. J. Lei, L. Li, R. Kostecki, R. Muller, and F. McLarnon, *J. Electrochem. Soc.*, **152**, A774 (2005).
22. M. Matsui, K. Dokko, and K. Kanamura, *J. Electrochem. Soc.*, **157**, A121 (2010).
23. F. Simmen, A. Hintennach, M. Horisberger, T. Lippert, P. Novák, C. W. Schneider, and A. Wokaun, *J. Electrochem. Soc.*, **157**, A1026 (2010).
24. F. Simmen, A. Foelske-Schmitz, P. Verma, M. Horisberger, Th. Lippert, P. Novák, C. W. Shneider, and A. Wokaun, *Electrochim. Acta*, **56**, 8539 (2011).
25. J. Hwang and H. Jang, *J. Electrochem. Soc.*, **162**, A103 (2015).
26. Y.-M. Liu, B. G. Nicolau, J. L. Esbenshade, and A. A. Gewirth, *Anal. Chem.*, **88**, 7171 (2016).
27. M. Mohamedi, D. Takahashi, T. Itoh, and I. Uchida, *Electrochim. Acta*, **47**, 3483 (2002).
28. A. Würsig, H. Buqa, M. Holzapfel, F. Krumeich, and P. Novák, *Electrochem. Solid-State Lett.*, **8**, A34 (2005).
29. M. Murakami, S. Shimizu, Y. Noda, K. Takegoshi, H. Arai, Y. Uchimoto, and Z. Ogumi, *Electrochim. Acta*, **147**, 540 (2014).
30. D. Aurbach, A. Zaba, Y. Ein-Eli, I. Weissman, O. Chusid, B. Markovsky, M. Levi, E. Levi, A. Schechter, and E. Granot, *J. Power Sources*, **68**, 91 (1997).
31. T. Kawamura, S. Okada, and J. Yamaki, *J. Power Sources*, **156**, 547 (2006).
32. S. E. Sloop, J. B. Kerr, and K. Kinoshita, *J. Power Sources*, **119**, 330 (2003).
33. J. Inamoto, T. Fukutsuka, K. Miyazaki, and T. Abe, *ChemistrySelect*, **2**, 2895 (2017).
34. A. J. Bard and L. R. Faulkner, *Electrochemical Methods, Fundamentals and applications, 2nd edition*, Wiley, New York, pp. 785–805. Appendix B (2001).
35. Y. Matsuo, Y. Sugie, K. Sakamoto, and T. Fukutsuka, *J. Solid State Electrochem.*, **15**, 503 (2011).
36. I. Yamada, T. Abe, Y. Iriyama, and Z. Ogumi, *Electrochem. Commun.*, **5**, 502 (2003).
37. M. Matsui, K. Dokko, and K. Kanamura, *J. Power Sources*, **177**, 184 (2008).